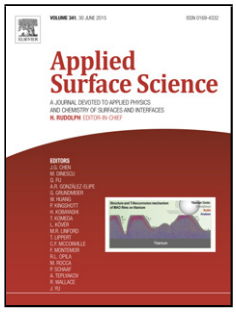

Title: A DFT Approach for Methanol Synthesis via Hydrogenation of CO on Gallia, Ceria and ZnO surfaces

Authors: Walter Reimers, Carolina Zubieta, Miguel Angel Baltanás, María Marta Branda

PII: S0169-4332(17)33692-9
DOI: https://doi.org/10.1016/j.apsusc.2017.12.104
Reference: APSUSC 37974

To appear in: *APSUSC*

Received date: 9-10-2017
Revised date: 8-12-2017
Accepted date: 12-12-2017

Please cite this article as: Reimers W, Zubieta C, Baltanás MA, Branda MM, A DFT Approach for Methanol Synthesis via Hydrogenation of CO on Gallia, Ceria and ZnO surfaces, *Applied Surface Science* (2010), https://doi.org/10.1016/j.apsusc.2017.12.104

A DFT Approach for Methanol Synthesis via Hydrogenation of CO on Gallia, Ceria and ZnO surfaces

Walter Reimers[a], Carolina Zubieta[b], Miguel Angel Baltanás.[c], María Marta Branda[a].

[a]IFISUR (UNS-CONICET), [b]INQUISUR (UNS-CONICET) Bahía Blanca, Argentina.
[c]INTEC (UNL-CONICET) Santa Fe, Argentina.

Graphical abstract

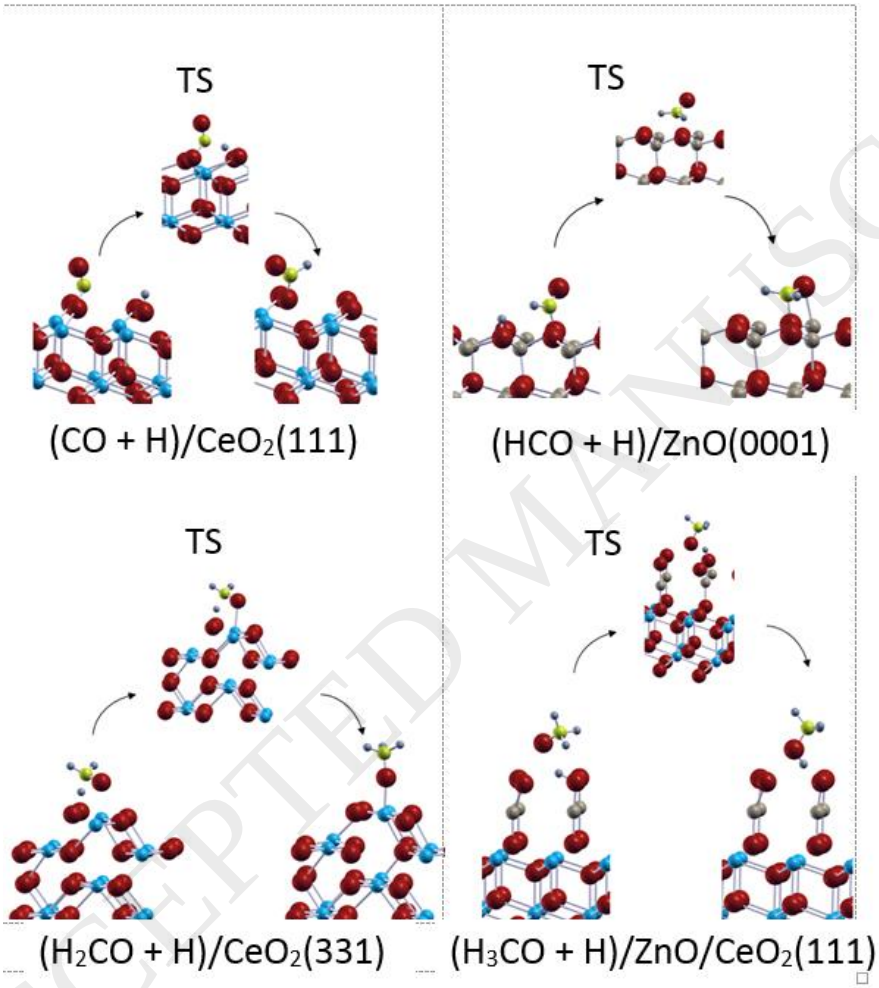

Highlights

- Highest activation barriers for reactions with significant geometric differences between initial and final configurations were found.
- The presence of superficial O vacancies promotes surface reactivity in the formation of intermediate species.
- Our results on surfaces with oxygen vacancies, especially ZnO (0001)vacO, are in line with current interest on these substrates in catalysis applications.
- Traditional BEP relationship (ΔE_{act} vs ΔE_{reac}) did not allow a good correlation to predict activation energy barriers.
- BEP relationships referred to the initial and/or final states, allowed to accurately find activation energy barriers.

Abstract

A systematic theoretical study of the consecutive hydrogenation reactions of the CO molecule for the methanol synthesis catalyzed by different oxides of Zn, Ce and Ga is reported in this work. First, the CO hydrogenation with the formation of formyl species (HCO) was analyzed, followed by the successive hydrogenations that lead to formaldehyde (H_2CO), methoxy (H_3CO) and, finally, methanol (H_3COH). The co-adsorption with H, in almost all the intermediate species, allows the corresponding hydrogenation reaction. Oxygen vacancies promote the reactivity in the generation of both formaldehyde and methoxy species. The formation of these species involves an important geometric difference between the initial and the final states, leading to high activation barriers. Comparing the surfaces studied in this work, we found that ZnO (0001)vacO has shown to be of a greater interest for methanol synthesis. However, the foregoing is not the most relevant of our results, but, instead, that the Brönsted Evans Polanyi (BEP) relationships between the initial or the final states and the transition states (TS) allowed to find a very good correlation between surface structure and reactivity.

Keywords: Methanol, CO, Hydrogenation, Oxides, DFT.

Introduction

Catalysts are used to increase the rate of a given chemical reaction. Despite the fact that the catalyst does not enter into the overall stoichiometric balance, its accelerating effect is generally due to the creation of an alternative reaction pathway- usually multistep -, which is characterized by a lower activation energy. Appropriate selection of the catalyst and reaction conditions make it possible to lead the reaction along a preselected pathway to yield the required product(s). The selectivity of a given catalyst depends mainly on the type of intermediates formed, and on their interactions with the surfaces exposed to the reacting media.

Nowadays the methanol synthesis, starting from $CO/CO_2/H_2$ gas mixtures, is a very important catalytic process [1]. Methanol, which is technological and industrially relevant for the synthesis of several chemical compounds, is expected to play a key role in the next generation of renewable energy sources to be used in fuel cells [2,3] and, also, as an intermediate for H_2 storage and transportation. Efficient dissociation of the H_2 molecule is usually carried out by a highly dispersed metal supported on a metal oxide, onto which – in most cases- CO hydrogenation proceeds.

In a recent study, Kattel et al. [4] made a direct comparison between the activity of two model catalysts, ZnCu and ZnO/Cu, to obtain more insight about the performance of the contemporary industrial catalyst for methanol synthesis, composed by Cu/ZnO/alumina, which is not as efficient as it would be desirable. By combining x-ray photoemission spectroscopy, density functional theory, and kinetic Monte Carlo simulations, they found a synergic effect in an interface made by ZnO/Cu that will enable the design of new catalysts which will save energy by working at lower temperatures and pressure.

Stampfl et al. [5] studied the reactivity and reaction pathways of various intermediates during the synthesis of methanol on thepolar ZnO (0001) surface by performing DFT calculations. They investigated the effect of surface coverage and found that a low coverage is energetically more favorable. The ZnO (0001) surface with oxygen vacancies was studied by Kiss et al. [6] to characterize molecular adsorption during methanol synthesis. They found that O defects are active sites for both CO and H_2 activation. CO interacts strongly with oxygen vacancies on the ZnO (0001) surface, in particular at F^{2+} sites. When ZnO is used as the catalyst support, there are still some unanswered questions about the reaction mechanism that yields methanol. Under high-pressure conditions, methanol is formed from CO on Cu-free ZnO catalysts [7], but some experimental data indicate that CO_2 is the primary carbon source for generating alcohol on $Cu/ZnO/Al_2O_3$ [8].

Likewise, in the last few years, there have been many studies of several aspects of bulk ceria and the reactivity of ceria surfaces, from both theoretical and experimental perspectives [9-19]. Fabris et al. studied the adsorption and oxidation of CO on CeO_2 (111) and (110) by means of DFT+U calculations. They found that the CO molecule is physisorbed on the (111) face and chemisorbed on

the (110) face of ceria [20]. The authors attributed this behavior to the formation of intermediate CO_x complexes.

Several workers have been suggesting different reaction pathways to obtain methanol via hydrogenation of CO and CO_2 [6,21-26]. It is well known that the alcohol synthesis on oxides proceeds following different reaction mechanisms than onto metallic surfaces. Experiments with tracer isotopes have made it clear that under commercial conditions for synthesizing methanol from $CO/CO_2/H_2$ mixtures, 70% of the preferred source of carbon –at least in the case of Cu-based catalyst - comes from CO_2 [8,27,28]. Therefore, the CO_2 molecule would appear to be a more important carbon source than CO for the alcohol synthesis on these materials. Nonetheless, Yang et al. studied the methanol synthesis with $CO/CO_2/H_2$ mixtures on Cu based catalysts by means of Fourier Transform Infrared (FTIR) spectroscopy and found that the main carbon source was not exclusive of CO or CO_2 but, rather, it depended on operating temperature. For elevated temperatures (higher than 453 K) CO_2 was the main source of carbon, whereas at lower temperatures (lower than 453 K) the carbon source was CO.

Considering the importance and desirability of having catalytic processes able to operate at low temperatures, and the fact that the commercial synthesis of methanol still take place around 523 K, the interest of the present paper is oriented to the hydrogenation of CO to methanol on different oxides of Zn, Ce and Ga. The latter oxide was chosen because of recent reports about its excellent performance as promoter of active, and selective novel catalysts for methanol synthesis from carbon oxide(s) mixtures [29,30].

The systematic analysis of the relative capacity of the studied oxides to carry out the synthesis of methanol from the CO and H_2 molecules represents a tool for both the design of new catalysts and the improvement *in silico* of their performances. So, the primary aim of this article is to quantify the reaction energies and activation barriers involved in the successive CO hydrogenation reactions that occur until the formation of methanol. In this way, our first goal is to be able to identify the best oxide surface to improve the selective hydrogenation of the carbon oxide. Following the systematic study of the adsorption of H_2, CO and CO_2 species on the same surface oxides reported by Reimers et al. [31], this work was also undertaken to help in providing a firm foundation for novel process development in methanol synthesis from carbon oxides, steam reforming of methanol for hydrogen production, and/or the water-gas shift reaction.

Computational details

Spin polarized density functional calculations (DFT) for periodic supercells representing different oxide surfaces were performed using the Vienna Abinitio Simulation Program (VASP, version 5.2.11). The projector augmented wave (PAW) method [32] was used to represent the interaction between the valence electrons and the atomic cores considering explicitly the Ce (4f, 5s, 5p, 5d, 6s), O (2s, 2p), C (2s,2p), and H (1s) electrons as valence states. The one-electron states were expanded on a plane-wave basis set with a kinetic cutoff energy of 415 eV. A proper Monkhorst–Pack grid of special k-points was used for all calculations [33]. Said calculations have been carried out using the PW91 [34,35] form of the Generalized Gradient Approximation (GGA) corrected with the so called on-site Hubbard parameter (U) [36]. GGA averages the exchange correlation of the electronic interaction, but does not correct the non-physical interaction of electrons derived from classical Coulomb interelectronic repulsion. When the CeO_{2-x} with reduced Ce atoms is studied, the Ce-4f strongly localized band is partially occupied and therefore DFT describes poorly the electronic structure. Then, considering the strong localization of the 4f electrons at Ce^{+3}, all calculations were done using the local density approximation (LDA + U) to obtain the optimal geometry of the systems and the generalized gradient approximation (GGA + U) in order to calculate the energy and charge values, where U is the Hubbard parameter that penalizes double occupation of the 4f orbital [36,37]. The optimal values of the Hubbard parameters selected by the LDA + U and GGA + U calculations were U = 5 and U = 3, respectively, in agreement with previous DFT studies [15].

Taking into account that dispersion effects on these systems were negligible, these calculations were done without van der Waals correction.

The Zero Point Energy (ZPE) corrections in the hydrogenation energies of CO, CHO, CH_2O and CH_3O were analyzed. The differences found between the calculations with and without these corrections were negligible (lower than 0.005 eV). For this reason, it was possible to neglect these corrections in our results.

Climbing-image Nudged Elastic Band method (CI-NEB) [38] implemented in the VASP code was used to search the pathway of the minimum energy between the reactants and products. This method involves performing successive calculations to find the true transition state. The initial and final states were verified with all values of real vibrational frequencies and the transition states were verified obtaining a single imaginary vibrational frequency. This imaginary frequency must be associated to the movement of atoms within the meaning of reaction pathway.

Models

The oxide surfaces analyzed in this work were: ZnO(0001) (Fig. 1A), $ZnO/CeO_2(111)$ (Fig. 1B), $CeO_2(111)$(Fig. 1C), $CeO_2(331)$ (Fig. 1D), and $Ga_2O_3(100)$ (Fig. 1E). For the cases of ZnO (0001), CeO_2 (111) and Ga_2O_3 the respective surfaces with O vacancies were also studied, from now on named as ZnO(0001)vacO, $CeO_2(111)$vacO, and $Ga_2O_3(100)$vacO, respectively (not shown in

Fig. 1). All al them were selected because they are the most stable crystal surfaces [39-48]. In addition, the polar ZnO (0001) surface was selected due to its relevance to both methanol synthesis and the water-gas shift reaction [5]. Lastly, a monolayer of ZnO on CeO_2(111) was analyzed, to compare its reactivity with those of the pure oxides. The ZnO monolayer was placed on an optimized slab representing the CeO_2(111) surface. This monolayer was geometrically relaxed, together with the three nearest layers of CeO_2.

The size of the cell used to model the surface is determined by the size and shape of the molecule to be adsorbed and the surface coverage to be studied. In this work, the perfect surfaces of CeO_2(111) and CeO_2(111)vacO were represented by 2×2 slabs with 9 atomic layers, allowing the relaxation of the three uppermost layers. The perfect surface of CeO_2(331) was represented by a 2×1 slab with 18 atomic layers, and ZnO was represented by a 3×3 slab with 9atomic layers, being in these cases six and three uppermost layers relaxed, respectively. Finally, a slab with one layer of ZnO over the slab of CeO_2(111) was built to represent ZnO grown epitaxially on CeO_2(111). All the slab models were separated by a vacuum >14 Å. Imposing periodic boundary conditions on the electrostatic potential of an asymmetric slab could give rise to an artificial electric field across the slab. Therefore, because the slabs analyzed in this work are not symmetric, we carried out single-point calculations using dipole correction to analyze possible changes in the adsorption energy [49,50].

Results and discussion

As a starting point, the initial (IS) and final states (FS) of each hydrogenation reaction were geometrically optimized. The reaction energies were calculated for all the studied surfaces as follows:

1) $H+CO/surf \rightarrow HCO/surf$
   $E_{reac1}= E(HCO/surf)-E(H+CO/surf)$,

2) $H+HCO/surf \rightarrow H_2CO/surf$
   $E_{reac2}= E(H_2CO/surf)-E(H+HCO/surf)$,

3) $H+H_2CO/surf \rightarrow H_3CO/surf$
   $E_{reac3}= E(H_3CO/surf)-E(H+H_2CO/surf)$,

4) $H+H_3CO/surf \rightarrow H_3COH/surf$
   $E_{reac4}= E(H_3COH/surf)-E(H+H_3CO/surf)$,

where H+CO/surf, H+HCO/surf, $H+H_2CO$/surf and $H+H_3CO$/surf correspond to the co-adsorption of H and CO, H and HCO, H and H_2CO, H and H_3CO on vicinal sites of the surface, respectively. At this point it is necessary to clarify that we considered only the simplest hydrogenation reactions. The existence of other more complex

reaction pathways are also possible, but they have not been studied until now. From the IS and FS, the minimal energy pathway and the corresponding TS were found (Figs. 2A-2D). In almost all the surfaces the formation of formyl (HCO) and methoxy (H_3CO) species involves similar IS and TS configurations (see Figs. 2A and 2C). The hydrogenation that leads to the formation of methanol presents TS and FS analogous configurations as well (Fig. 2D). However, the geometric difference between the IS, TS and FS in the case of the reactions to form formaldehyde is significant, as it can be appreciated in Fig. 2B.

An alternative way to find more easily the TS was explored. So, in order to find all the activation energy values the Brönsted Evans Polanyi (BEP) method was used. The traditional lineal-BEP relation is defined as

$$E_{act} = \alpha E_{reac} + \beta \quad (1)$$

The objective was to find a linear relationship between the activation and reaction energies, from the values previously found with the NEB method, for each of the four hydrogenation reactions on every studied surfaces. The activation and reaction energy values for each hydrogenation reaction on the oxide surfaces are jointly indicated in Fig. 3A. As it can be observed, the web of points does not fit a linear relationship, except for the case of the formation of methoxy. The BEP traditional equation for the formation of methoxy species is separately displayed in Fig. 3B (correlation coefficient, r^2=0.96). Plausibly, these results might be due to different geometric changes in the other reactions, where in some of them the IS and TS are similar but not in the others. Even so, Fig. 3A indicates that 75% of the reactions studied are exothermic.

Despite this initial setback, it was still possible to resort to some other linear relationships that enabled us to predict the absent activation energies. For example, Fajin et al. [51] found a linear relationship for the dissociation of CH_3OH on different metal surfaces in terms of descriptors such as the co-adsorption energy for CH_3O and H species and also descriptors in terms of the energy of adsorption of one O atom. Other authors, as Wang et al. [52], studying the surfaces of transition metals, have found linear relationships with descriptors in terms of the dissociation energy of the CH_4, H_2O, NH_3 and H_2 molecules. Lee et al. [53] considered descriptors in terms of the relative energy for initial and final states, in a DFT study for dissociation reactions of C-H, O-H, C-C, C-O and C-OH on bimetallic surfaces of Rh-Ni.

Likewise, Vojvodic et al. [54] proved that it is possible to build BEP relationships for transition metal oxides as well, which are strongly dependent on the dissociation of the molecule and/or surface reactivity linking properties. Then, several descriptors taken from these research teams were tried in this work. With respect to the initialand final states, transition state energies can be defined as

$$\Delta E_{TS} = \alpha \Delta E_{initial} + \beta \quad (2)$$

$$\Delta E_{TS} = \alpha' \Delta E_{final} + \beta' \quad (3)$$

respectively, where:

$$\Delta E_{TS} = E_{TS} - E_{molecule} - E_{surface} \quad (4)$$

$$\Delta E_{initial} = E_{initial} - E_{molecule} - E_{surface} \quad (5)$$

$$\Delta E_{final} = E_{final} - E_{molecule} - E_{surface} \quad (6)$$

$E_{initial}$, E_{TS} and E_{final} are the total energies of the initial, transition and final states respectively and $E_{molecule}$ is the total energy of the gas molecule(s), in our case CO plus a fraction of H_2. For the hydrogenation reaction of CO leading to formyl formation (Fig. 4A and 4B) both descriptors are acceptable, because they have similar correlation coefficients. For the reaction of formyl hydrogenation (formaldehyde formation) a low value of the correlation coefficient, r^2= 0.762, was found using the relative descriptor for initial state (figure not shown). Certainly, this is the only possible descriptor for this reaction. For the hydrogenation of formaldehyde an acceptable fitting with the descriptors relative to the final state was found (figure not shown). This fitting, together with the one obtained from traditional BEP constituted good approaches to find the absent transition state energies (i.e., the sought-after activation barriers). In Figs. 4C and 4D the descriptors referred to the initial and final configurations, respectively, are displayed for the reaction step of methanol formation. In both cases, we obtained a high correlation coefficient of around 0.99, being both excellent predictors for the interpolation needed to obtain the activation barriers. Finally, the BEP relationship for all of the reaction steps on the set of studied oxides, with descriptors referred to both initial and final states, are displayed in Fig. 5. The fitting found using the BEP method with a descriptor relative to the initial energy was more suitable. Herein, we highlight the following descriptors because they have shown acceptable linear relationships for future predictions:

1) Formation of formyl (HCO)

Relative to the initial state: $\Delta E_{TS} = 0.92\Delta E_{initial} + 0.55$ (7)

Relative to the final state: $\Delta E_{TS} = 1.06\Delta E_{final} + 1.17$ (8)

2) Formation of formaldehyde (H_2CO)

Relative to the initial state: $\Delta E_{TS} = 0.73\Delta E_{initial} + 0.99$ (9)

3) Formation of methoxy (H_3CO)

Traditional BEP: $\Delta E_{activation} = 0.85\Delta E_{reaction} + 1.75$ (10)

Relative to the final state: $\Delta E_{TS} = 0.67\Delta E_{final} + 1.12$ (11)

4) Formation of methanol (H_3COH)

Relative to the initial state: $\Delta E_{TS} = 1.07\Delta E_{initial} + 0.56$ (12)

Relative to the final state: $\Delta E_{TS} = 1.41\Delta E_{final} + 1.19$ (13)

Using these BEP-derived relationships we can predict the values of the needed activation energies that could not be found by both the NEB method and traditional BEP equations. For that purpose we used the predictors 7-13 as appropriate. Inputting known values in the x-axis, either $E_{reaction}$, $\Delta E_{initial}$ or ΔE_{final}, and by means of equations 14 to 25 (see below) we calculated the whole set of energy barriers:

1) Formation of formyl (HCO)

$$\Delta E_{initial}(HCO) = E_{initial}(HCO) - ECO_{gas} - \frac{1}{2}EH_{2\,gas} - E_{surface} \quad (14)$$

$$\Delta E_{TS}(HCO) = E_{TS}(HCO) - ECO_{gas} - \frac{1}{2}EH_{2\,gas} - E_{surface} \quad (15)$$

$$\Delta E_{final}(HCO) = E_{final}(HCO) - ECO_{gas} - \frac{1}{2}EH_{2\,gas} - E_{surface} \quad (16)$$

where $E_{initial}$, E_{TS}, E_{final} are the IS, TS and FS energies, respectively, for the first hydrogenation step: formyl formation from CO and ½ H_2. ECO_{gas}, and $EH_{2\,gas}$ are the energies of the free CO and H_2 molecules.

2) Formation of formaldehyde (H_2CO)

$$\Delta E_{initial}(H_2CO) = E_{initial}(H_2CO) - EH_2CO_{gas} - E_{surface} \quad (17)$$

$$\Delta E_{TS}(H_2CO) = E_{TS}(H_2CO) - EH_2CO_{gas} - E_{surface} \quad (18)$$

$$\Delta E_{final}(H_2CO) = E_{final}(H_2CO) - EH_2CO_{gas} - E_{surface} \quad (19)$$

where $E_{initial}$, E_{TS}, E_{final} are the energies of IS, TS and FS, respectively, for formaldehyde formation and EH_2CO_{gas} is the energy of the free H_2CO molecule.

3) Formation of methoxy (H_3CO)

$$\Delta E_{initial}(H_3CO) = E_{initial}(H_3CO) - ECO_{gas} - \frac{3}{2}H_{2\,gas} - E_{surface} \quad (20)$$

$$\Delta E_{TS}(H_3CO) = E_{TS}(H_3CO) - ECO_{gas} - \frac{3}{2}H_{2\,gas} - E_{surface} \quad (21)$$

$$\Delta E_{final}(H_3CO) = E_{final}(H_3CO) - ECO_{gas} - \frac{3}{2}H_{2\,gas} - E_{surface} \quad (22)$$

where $E_{initial}$, E_{TS}, E_{final} are the energies of IS, TS and FS, respectively, for the hydrogenation of formaldehyde to adsorbed methoxy and ECO_{gas} and $EH_{2\,gas}$ are the energies of the CO and H_2 free molecules.

4) Formation of methanol (H_3COH)

$$\Delta E_{initial}(H_3COH) = E_{initial}(H_3COH) - EH_3COH_{gas} - E_{surface} \quad (23)$$

$$\Delta E_{TS}(H_3COH) = E_{TS}(H_3COH) - EH_3COH_{gas} - E_{surface} \quad (24)$$

$$\Delta E_{final}(H_3COH) = E_{final}(H_3COH) - EH_3COH_{gas} - E_{surface} \quad (25)$$

where$E_{initial}$, E_{TS}, E_{final} are the energies of IS, TS and FS, respectively, for the final hydrogenation of methoxy to methanol and EH_3COH_{gas} is the energy of free methanol molecule.

Reaction and activation energies for the formation of each intermediate on the different oxide surfaces are reported in **Table 1**, where the regular and boldface values correspond to the activation barriers found by NEB and by interpolation, respectively. For the case of the interpolated values, where more than one predictor is possible, the value calculated with the predictor of highest coefficient of correlation was reported first.

As it can be observed from **Table 1**, when two predictors were used the obtained results were similar, with the lowest difference between them (0.05 eV) for the reaction methoxy-methanol on the CeO_2 (111)vacO surface, and the highest (0.4 eV) for the formation of methoxy on the perfect surface of ZnO (0001). An exception occurred for the interpolation in the methoxy formation reaction on Ga_2O_3 (100)vacO. With one of the predictors (traditional BEP) a value of 0.12 eV was obtained, whereas with the final state predictor the value was -0.60 eV instead. Taking into account that the values of energy barrier cannot be negative, this singularity might be explained based on the significantly difference between the energy of the final state energy and the energy of the transition state. In addition, their respective geometries are also very different.

Be that as it may, it is worth to note that the highest values of activation energy barriers corresponded to the reactions of hydrogenation of formyl and formaldehyde on perfect surfaces. The highest values occurred in ZnO (0001), being 3.05 eV for formaldehyde formation and 4.50 eV for the methoxy formation. The hydrogenation reactions leading to formation of formaldehyde and/or methoxy on these perfect surfaces constituted the determining step for the synthesis of methanol. The other reactions (formyl and methanol formation) have smaller barriers. Also, it should be underlined that the barriers for formation of

formaldehyde and methoxy decrease considerably when the surface has oxygen deficiency. The lowest energetic barriers were found for the formation reaction of formyl and methanol, on each of the studied surfaces.

Reactivity trends.

From the former analyses, for all the studied hydrogenation reactions the corresponding reaction pathways were built. The hydrogenation of CO to formyl on the perfect surfaces: ZnO (0001), CeO_2 (111), CeO_2 (331) and Ge_2O_3 is displayed in Fig. 6A. The same reaction on ZnO (0001)vacO, CeO_2 (111)vacO, Ga_2O_3 (100)vacO and ZnO/CeO_2 (111) is shown in Fig 6B.

The zero energy reference was computed with respect to free gaseous species (CO and H_2) (see Eqs. 14 to 16). In this way, the zero point of energy corresponds to: E_{surf} + E(CO) + ½ E(H_2) (black line in the graphic).

As it can be observed, this reaction is exothermic on the perfect surfaces and also on the surfaces with O vacancies. However, it is endothermic on ZnO/CeO_2 (111).

The highest activation barriers -around 1 eV -, were found on Ga_2O_3 (100), Ga_2O_3 (100)vacO and ZnO/CeO_2 (111). For the other surfaces these barriers are smaller than 0.5 eV. Although the activation barriers on CeO_2 (111), ZnO (0001)vacO and CeO_2 (111)vacO are lower than 0.5 eV, this reaction is scrolled left; that is, regenerating the reagents instead of progressing to the final state (formyl).

On ZnO (0001), Ga_2O_3 (100) and ZnO/CeO_2 (111) the reaction is displaced instead to the final state, even though the barriers on Ga_2O_3 (100) and ZnO/CeO_2 (111) are around 1.2 eV. Finally, on CeO_2 (331) the activation barrier is small and the reaction is significantly exothermic.

The hydrogenation of HCO to formaldehyde on the perfect surfaces: ZnO (0001), CeO_2 (111), CeO_2 (331) and Ga_2O_3 (100) is described in Fig. 7A. The same reaction on ZnO (0001)vacO, CeO_2 (111)vacO, Ga_2O_3 (100)vacO and ZnO/CeO_2 (111) is shown in Fig 7B. The reaction is exothermic on Ga_2O_3 (100), Ga_2O_3 (100)vacO and CeO_2 (111)vacO and endothermic on ZnO (0001) and ZnO (0001)vacO. Comparing the perfect surfaces with the respective ones with O vacancies, a remarkable decrease in the energy barriers of the latter was found.

To analyze the preferred direction of the reaction, a similar study as the one for the formation of formyl species was made. From Eqs. 17 to 19 the tendency of the reaction with respect to the final state was analyzed. Here, the 'zero' point of energy corresponds to: $E_{surf} + E(H_2CO)$. As it can be observed in Fig. 7, both on the bare and/or with O-vacancy surfaces (Ga_2O_3 (100), CeO_2 (111), ZnO (0001)vacO, CeO_2 (111)vacO and Ga_2O_3 (100)vacO) the reaction trend is toward the products. However, only the CeO_2 (111) and Ga_2O_3 (100)vacO surfaces exhibit energy barriers lower than 1 eV. On the epitaxial ZnO/CeO_2 surface the reaction is displaced to the reactants, with a small activation barrier. Noteworthily, the energetic requirement from the final state (CH_2O_{surf}) to the 'zero' (CH_2O_{gas} + surface) is around 3 eV. However, the reverse energy barrier in order to return to

the initial state is lower than 1eV. On the ZnO (0001) and CeO_2 (331) surfaces the tendency toward products or reactants is the same, because the energy of transition state is close to that of the products.

The energy diagram for the formation of methoxy from H_2CO hydrogenation on the perfect surfaces: ZnO (0001), CeO_2 (111), CeO_2 (331) and Ga_2O_3 (001) is displayed in Fig. 8A. The same reaction on ZnO (0001)vacO, CeO_2 (111)vacO, Ga_2O_3 (100)vacO and ZnO/CeO_2 (111) is shown in Fig. 8B. All the reactions on the surfaces with O vacancies are exothermic, while on the other ones are endothermic. It is apparent, then, that the presence of superficial O vacancies produces a considerable decrease in the activation barriers for this reaction. For this intermediate species, methoxy, the reference energy with respect to the reactants was: CO + 3/2 H_2. The zero point of energy corresponds to $E_{surf} + E(CO) + 3/2\, E(H_2)$ (see Eqs. 20 to 22). On ZnO (0001) and Ga_2O_3 (100)vacO the reaction is displaced towards the formation of reactants, although the energy barrier for the case of gallia is small (<0.5 eV). Conversely, on ZnO (0001)vacO and CeO_2 (111)vacO (both exhibiting small activation barriers), the opposite occurs. No particular tendency could be appreciated for CeO_2 (111), CeO_2 (331) and Ga_2O_3 (100).

Finally, the energy diagram for the hydrogenation of H_3CO to methanol on the perfect surfaces: ZnO (0001), CeO_2 (111), CeO_2 (331) and Ga_2O_3, is presented in Fig. 9A. For clarity purposes, the same reaction on ZnO (0001)vacO, CeO_2 (111)vacO, Ga_2O_3 (100)vacO and ZnO/CeO_2 (111) is shown in Fig. 9B.

On ZnO(0001) and Ga_2O_3 (100)vacO, the reactions are exothermic, being slightly so on CeO_2 (111), ZnO/CeO_2 (111) and CeO_2 (111)vacO. However, on CeO_2 (331), Ga_2O_3 (100) and ZnO (0001)vacO the reaction is slightly endothermic. The activation barriers reported for methoxy hydrogenation are smaller than for the previous species. This might be possible because of in this last hydrogenation (methoxy to methanol) the geometric configurations of the initial and the final states are only slightly different.

The energy diagram for this reaction was referenced to the final state. The zero point of energy corresponds to: $E_{surf} + E(H_3COH)$ (see Eqs. 23 to 25). As it can be observed in Figs. 9A and B, on the ZnO (0001), ZnO/CeO_2 (111) and Ga_2O_3 (100)vacO surfaces this reaction favors the products, with the smaller barrier for ZnO (0001). On the contrary, the reaction on CeO_2 (111), CeO_2 (331), Ga_2O_3 (100) and both ZnO (0001)vacO and CeO_2 (111)vacO shows displacement toward the reagents.

Potential energy surfaces

Up to now an energetic analysis of the separate formation of each intermediate species and the final CO hydrogenation product, methanol, was made. In this way, the energy of the species that may exist in gas phase (i.e. formaldehyde and methanol) was defined based on the final configuration for the respective reaction

step, while those species that exist as radicals (surface adsorbate) were referred to the initial constituents of the hydrogenation process (CO and H_2).

To have a more complete vision of the relative stabilities of the formed species throughout the complete hydrogenation process on each surface, the relative energies vs. reaction coordinate were displayed in Figs. 10 to 12. Here, the same reference energy for all the dehydrogenation reaction steps was take,, which was defined as: $E_{zero} = E_{surf} + E(2H_2) + E(CO)$, where E_{surf} stands for the free surface energy, E ($2H_2$) is the energy of two H_2 molecules and E (CO) is the energy of the CO molecule, both in the gas phase.

For the purpose of completing the total amount of the 4H involved in the alcohol synthesis we added to the corresponding adsorbate or product, for each surface and each hydrogenation step, the energy of the H_2 fraction involved, namely: For formyl formation: + $E(3/2\ H_2)$, for formaldehyde formation: $+E(H_2)$, for methoxy formation: + $E(1/2\ H_2)$, and for methanol: +0.

So, it can be readily appreciated that for ZnO (0001), ZnO (0001)vacO and ZnO/Ceria(111) the co-adsorption of each of the intermediate species and a neighbor hydrogen is favored. However, the largest quantum wells (i.e., where there is a major stability), correspond to the hydrogenation steps leading to formyl and formaldehyde co-adsorbed with a H atom. For the case of the generation of methoxy on ZnO/CeO_2, the co-adsorption with H was slightly unstable. The formation of the formaldehyde and methoxy intermediates are the most energetically demanding steps on both the perfect ZnO (0001) and the ZnO (0001)vacO surfaces. From these figures we can observe that the latter is the most favorable surface for all the hydrogenation reactions. However, both ZnO (0001) and ZnO/Ceria(111) surfaces show transition state energies (formation of methoxy and methanol, respectively) higher than the initial separate systems energy, indicating a major stability of formyl and formaldehyde species.

The two perfect surfaces of CeO_2 and CeO_2 (111)vacO are shown in Figs. 11A-C. In the three surfaces greater energetic stability for the methoxy co adsorption with an H atom, was found. Again, it can be appreciated that the presence of oxygen vacancies, now in CeO_2 (111), turns the surface more reactive. From these figures it could also be inferred that the most likely species on the perfect Ceria surfaces are HCO and H_2CO while in the case of CeO_2-vacO surface are CO and HCO.

In Fig 12 the reactivity of the perfect Ga_2O_3 (100) and Ga_2O_3 (100)vacO surfaces is shown. In either case the co adsorption with H did not increase the stability of the adsorbed species. In addition, the reactivity of Gallia does not increase when O vacancies are present.

Conclusions

The sequential hydrogenation reactions undergone by the CO molecule for methanol synthesis on different oxides of Zn, Ce and Ga were studied by DFT calculations. Our main findings were the following:

- The higher activation barriers for the formation of the formaldehyde and methoxy surface intermediates are probably due to the significant geometric difference between their initial and final configurations.
- The presence of superficial O vacancies for all the studied oxides promote the reactivity in the formation of both the formaldehyde and methoxy species.
- "Surfaces with oxygen vacancies, ZnO (0001)vacO and CeO_2 (111)vacO, as well as stepped CeO_2 (331), have shown a reactivity enhancement with respect to the perfect ones".
- The traditional BEP relationship (ΔE_{act} vs ΔE_{reac}) did not allow a good correlation to predict activation energy barriers. However, BEP relationships referred to the initial and/or final states allowed to find them satisfactorily.
- No preference between the initial and final descriptors for the activation energies calculation was observed. Although in some reactions a good descriptor was found for the initial state reference, the situation was the opposite in other cases.

We hope that the present findings might stimulate further theoretical and/or experimental investigation about the synthesis of methanol. We found trends and preferences in the reaction pathways leading to the different intermediates, which may allow in the design and optimization of novel, more efficient catalysts. This would then enable, a less energy-intensive production of this alcohol. Being a clean fuel, methanol may positively contribute to a significant reduction of contamination at a global scale.

Acknowledgements

This research was carried out with the financial support of CONICET – Argentina (PIP 112-2010100949), ANPCyT – Argentina (PICT 2010 - N_ 0830) and Universidad Nacional del Sur – Argentina (PGI – UNS N_ 24/F051). MAB thanks Universidad Nacional del Litoral (UNL) and CONICET for their continued support.

Surface	*Formation of*	*E react (eV)*	*E act (eV)*
ZnO(0001)	*Formyl*	-0.64	0.14
	Formaldehide	2.83	3.05
	Methoxy	3.34	**4.50 / 4.10**
	Methanol	-0.91	0.4
ZnO(0001)vacO	*Formyl*	-0.84	0.1
	Formaldehide	1.55	2.01
	Methoxy	-1.27	0.37
	Methanol	0.45	**0.65 / 0.45**
ZnO/CeO_2(111)	*Formyl*	1.31	1.24
	Formaldehide	-0.09	0.48
	Methoxy	-----	-----
	Methanol	-0.22	0.9
CeO_2(111)	*Formyl*	-1.59	0.14
	Formaldehide	-0.23	2.97
	Methoxy	0.5	2.15
	Methanol	-0.05	0.13
CeO_2(111)vacO	*Formyl*	-0.43	**0.52 / 0.72**
	Formaldehide	-1.59	0.89
	Methoxy	-2.1	0.19
	Methanol	-0.72	**0.24 / 0.29**
CeO_2(331)	*Formyl*	-1.31	0.17
	Formaldehide	-0.02	**1.29**
	Methoxy	0.58	2.36
	Methanol	0.3	0.51
Ga_2O_3(100)	*Formyl*	-0.09	1.21
	Formaldehide	-3.69	1.37
	Methoxy	1.1	**2.68/2.55**
	Methanol	0.49	**0.60**
Ga_2O_3(100)vacO	*Formyl*	-0.33	1,05
	Formaldehide	-3.28	0.39
	Methoxy	-1.92	**0.12/-0.60**
	Methanol	*-0.75*	*0.7*

Table 1: Reaction (E_{react}) and activation (E_{act}) energies for the formation of each intermediate species on the different oxide surfaces, where the regular and boldface values correspond to the activation barriers found by NEB and by interpolation, respectively.

References

[1] G. Zahedi, A. Elkamel, A. Lohi, A. Jahanmiri, M.R. Rahimpour, Hybrid artificial neural network—First principle model formulation for the unsteady state simulation and analysis of a packed bed reactor for CO_2 hydrogenation to methanol, Chem. Eng. J. 115 (2005) 113-120.

[2] S. Sá, H. Silva, L. Brandao, J.M. Sousa, A. Mendes, Catalysts for methanol steam reforming, Appl. Catal. B: Environ. 99 (2010) 43-57.

[3] W. D. Hsu, T. Ichihashi, T. Kondow, S. B. Sinnot, Ab initio molecular dynamics study of methanol adsorption on copper clusters, J. Phys. Chem. A 111 (2007) 441–449.

[4] S. Kattel, P. J. Ramírez, J. G. Chen, J. A. Rodríguez, P. Liu, Active sites for CO_2 hydrogenation to methanol on Cu/ZnO catalysts, Science 355 (2017) 1296–1299.

[5] K. Chuasiripattana, O. Warschkow, B. Delley, C. Stampfl, Reaction intermediates of methanol synthesis and the water–gas-shift reaction on the ZnO(0001) surface, Surf. Sci. 604 (2010) 1742-1751.

[6] J. Kiss, J. Frenzel, B. Meyer, D. Marx, Methanol synthesis on ZnO(0001). II. Structure, energetic, and vibrational signature of reaction intermediates, J. Chem. Phys. 139 (2013) 1–17.

[7] M. Kurtz, J. Strunk, O. Hinrichsen, M. Muhler, K. Fink, B. Meyer, C. Wöll, Aktivezentren an oxidoberflächen: Die ZnO-katalysierte methanol-synthese, Angew. Chem. 117 (2005) 2850-2854.

[8] G. C. Chinchen, P. J. Denny, D. G. Parker, M. S. Spencer, D. A. Whan, Mechanism of methanol synthesis from $CO_2/CO/H_2$ mixture over copper/zinc oxide/alumina catalysts, Appl. Catal. 30 (1987) 333-338.

[9] J. C. Conesa, Computer modeling of surfaces and defects on cerium dioxide, Surf. Sci. 339 (1995) 337–352.

[10] S. Gennard, F. Cora, C. R. A. Catlow, Comparison of the bulk and surface properties of ceria and zirconia by ab initio investigations, J. Phys. Chem. B 103 (1999) 10158–10170.

[11] N. Skorodumova, M. Baudin, K. Hermansson, Surface properties of ceria from first principles, Phys. Rev. B 69 (2004) 1–8.

[12] P. J. Hay, R. L. Martin, J. Uddin, G. E. Scuseria, Theoretical study of CeO_2 and Ce_2O_3 using a screened hybrid density functional, J. Chem. Phys. 125 (2006) 1–8.

[13] H-T. Chen, Y. M. Choi, M. Liu, M. C. Lin, A theoretical study of surface reduction mechanisms of CeO_2(111) and (110) by H_2, Chem. Phys. Chem. 8 (2007) 849–855.

[14] J. L. F. Da Silva, M. V. Ganduglia-Pirovano, J. Sauer, V. Bayer, G. Kresse, Hybrid functionals applied to rare-earth oxides: the example of ceria, Phys. Rev. B 75 (2007) 1–10.

[15] C. Loschen, J. Carrasco, K. M. Neyman, F. Illas, First principles LDA + U and GGA + U study of cerium oxides: dependence on the effective U-parameter, Phys. Rev. B 75 (2007) 031151-1–03115-8.

[16] C. W. M. Castleton, J. Kullgren, K. Hermansson, Tuning LDA + U for electron localization and structure at oxygen vacancies in ceria, J. Chem. Phys. 127 (2007) 1–11.

[17] M. M. Branda, C. Loschen, K. M. Neyman, F. Illas, Atomic and electronic structure of cerium oxide stepped model surfaces, J. Phys. Chem. C 112 (2008) 17643–17651.

[18] A. M. Burow, T. Wende, M. Sierka, R. Włodarczyk, J. Sauer, P. Claes, L. Jiang, G. Meijer, P. Lievens, K. R. Asmis, Structures and vibrational spectroscopy of partially reduced gas-phase cerium oxide clusters, Phys. Chem. Chem. Phys. 13 (2011) 19393–19400.

[19] D. Lu, P. Liu, Rationalization of the Hubbard U parameter in CeO_x from first principles: unveiling the role of local structure in screening, J. Chem. Phys. 140 (2014) 1–7.

[20] M. Huang, S. Fabris, CO adsorption and oxidation on ceria surfaces from DFT + U calculations, J. Phys. Chem. C 112 (2008) 8643–8648.

[21] L. C. Grabow, M. Mavrikakis, Mechanism of methanol synthesis on Cu through CO_2 and CO hydrogenation, ACS Catal. 1 (2011) 365-384.

[22] C. T. Vo, L. K. Huynh, J-Y. Hung, J-C. Jiang, Methanol adsorption and decomposition on ZnO(1010) surface: A density functional theory study, Appl. Surf. Sci. 280 (2016) 219-224.

[23] Y. Yang, C. A. Mims, D. H. Mei, C. H. F. Peden, C. T. Campbell, Mechanistic studies of methanol synthesis over Cu from $CO/CO_2/H_2/H_2O$ mixtures: The source of C in methanol and the role of water, J. Catal. 298 (2013) 10-17.

[24] I. N. Remediakis, F. Abild-Pedersen, J. K. Norskov, DFT Study of formaldehyde and methanol synthesis from CO and H_2 on Ni(111), J. Phys. Chem. B 108 (2004) 14535–14540.

[25] J. Kiss, J. Frenzel, N. N. Nair, B. Meyer, D. Marx, Methanol synthesis on ZnO(0001). III. Free energy landscapes, reaction pathways, and mechanistic insights, J. Chem. Phys. 134 (2011) 64710-64714.

[26] Y-F. Zhao, R. Rosseau, J. Li, D. Mei, Theoretical study of syngas hydrogenation to methanol on the polar Zn-terminated ZnO(0001) surface, J. Phys. Chem. 116 (2012) 15952-15961.

[27] Y. B. Kagan, A. Y. Rozovskij, L. G. Liberov, E. V. Slivinskij, G. I. Lin, S. M. Loktev, A. N. Bashkirov, Study of mechanism of methanol synthesis from carbon monoxide and hydrogen using radioactive carbon isotope C14, Dokl. Akad. Nauk SSSR Ser. Khim. 224 (1975) 1081–1084.

[28] V. E. Ostrovskii, Mechanisms of methanol synthesis from hydrogen and carbon oxides at Cu–Zn-containing catalysts in the context of some fundamental problems of heterogeneous catalysis. Catal. Today 77 (2002) 141-160.

[29] T. Fujitani, M. Saito, Y. Kanai, Y. Watanabe, J. Nakamura, Y. Uchijima, Development of an active Ga_20_3 supported palladium catalyst for the synthesis of methanol from carbon dioxide and hydrogen, Appl. Catal. A Gen 125 (1995) 199-202.

[30] S. E. Collins, J. J. Delgado, C. Mira, J.J. Calvino, S. Bernal, D. L. Chiavassa, M. A. Baltanás, A. L. Bonivardi, The role of Pd–Ga bimetallic particles in the bifunctional mechanism of selective methanol synthesis via CO_2 hydrogenation on a Pd/Ga_2O_3 catalyst, J. Catal. 292 (2012) 90–98.

[31] W. R. Reimers, M. A. Baltanás, M. M. Branda, Theoretical study on the reactivity of the surface of pure oxides: The Influence of the support and oxygen vacancies, App. Surf. Sci. 274 (2013) 1-6.

[32] P. E. Blöchl, Projector augmented-wave method, Phys. Rev. B 50 (1994) 17953-17979.

[33] H. J. Monkhorst, J. D. Pack, Special points for Brillouin-zone integrations. Phys. Rev. B 13 (1976) 5188-5192.

[34] J. P. Perdew, J. A. Chevary, S. H. Vosko, K. A. Jackson, M. R. Pederson, D. J. Singh, C. Fiolhais, Atoms, molecules, solids, and surfaces: Applications of the generalized gradient approximation for exchange and correlation, Phys. Rev. B 46 (1992) 6671-6687.

[35] J. P. Perdew, J. A. Chevary, S. H. Vosko, K. A. Jackson, M. R. Pederson, D. J. Singh, C. Fiolhais, Erratum: Atoms, molecules, solids, and surfaces: Applications of the generalized gradient approximation for exchange and correlation, Phys. Rev. B 48 (1993) 4978-4984.

[36] V. I. Anisimov, F. Aryasetiawan, A. I. Lichtenstein, First-principles calculations of the electronic structure and spectra of strongly correlated systems: the LDA + U method, J. Phys. Condens. Matter 9 (1997) 767-808.

[37] S. L Dudarev, G. A. Botton, S. Y. Savrasov, C. J. Humphreys, A . P. Sutton, Electron-energy-loss spectra and the structural stability of nickel oxide: an LSDA+U study, Phys. Rev. B 57 (1998) 1505-1509.

[38] H. Jónsson, G. Mills, K. W. Jacobsen, Nudged elastic band method for finding minimum energy paths of transitions, Classical and Quantum Dynamics in Condensed Phase Simulations (1998) 385-404.

[39] N. N. Skorodumova, M. Baudin, K. Hermansson, Surface properties of CeO_2 from first principles, Phys. Rev. B 69 (2004) 075401-1-075401-8.

[40] B. Herschend, M. Baudin, K. Hermansson, Electronic structure of the CeO_2(110) surface oxygen vacancy, Surf. Sci. 599 (2005) 173-186.

[41] B. Herschend, M. Baudin, K. Hermansson, CO adsorption on CeO_2(110) using hybrid-DFT embedded-cluster calculations, Chem. Phys. 328 (2006) 345-353.

[42] K. Klier, Methanol synthesis, Adv. Catal. 31 (1982) 243-313.

[43] K. Teramura, H. Tsuneoka, T. Shishido, T. Tanaka, Effect of H_2 gas as a reductant on photoreduction of CO_2 over a Ga_2O_3photocatalyst, Chem. Phys. Lett. 467 (2008) 191-194.

[44] M. Calatayud, S. E. Collins, M. A. Baltanás, A. L. Bonivardi, Stability of formate species on β-Ga_2O_3, Phys. Chem. Chem. Phys. 11 (2009) 1397-1405.

[**45**] S. E. Collins, M. A. Baltanás, A. L. Bonivardi, An infrared study of the intermediates of methanol synthesis from carbon dioxide over Pd/β-Ga_2O_3, J. Catal. 2004, 226, 410-421.

[46] D. L. Chiavassa, J. Barrandeguy, A. L. Bonivardi, M. A. Baltanás, Methanol synthesis from CO_2/H_2 using Ga_2O_3-Pd/silica catalysts: Impact of reaction products, Catal. Today 133 (2008) 780-786.

[47] W. Jochum, S. Penner, R. Kramer, K. Föttinger, G. Rupprechter, B. Klötzer, Defect formation and the water–gas shift reaction on β-Ga_2O_3, J. Catal. 256 (2008) 278-286.

[48] S. E. Collins, M. A. Baltanás, A. L. Bonivardi, Infrared spectroscopic study of the carbon dioxide adsorption on the surface of Ga_2O_3 polymorphs, J. Phys. Chem. B 110 (2006) 5498-5507.

[49] J. Neugebauer, M. Scheffler, Adsorbate-substrate and adsorbate-adsorbate interactions of Na and K adlayers on Al(111), Phys Rev B 46 (1992) 16067–16080.

[50] G. Makov, M. C. Payne, Periodic boundary conditions in ab initio calculations, Phys Rev B 51 (1995) 4014–4022.

[51] J. L. C. Fajin, M. N. D. S. Cordeiro, F. Illas, J. R. B. Gomes, Generalized Brønsted–Evans–Polanyi relationships and descriptors for O–H bond cleavage of organic molecules on transition metal surfaces, J. Catal. 313 (2014) 24-33.

[52] S. Wang, V. Petzold, V. Tripkovic, J. Kleis, J. G. Howalt, E. Skulason, E. M. Fernandez, B. Hvolbaek, G. Jones, A. Toftelund, H. Falsing, M. Bjorketun, F. Studt, F. Abild-Pedersen, J. Rossmeisl, J. K. Norskov, T. Bligaard, Universal transition state scaling relations for (de)hydrogenation over transition metals, Phys. Chem. Chem. Phys. 13 (2011) 20760-20765.

[53] K. Lee, E. Lee, C. Song, M. J. Janik, Density functional theory study of propane steam reforming on Rh–Ni bimetallic surface: Sulfur tolerance and scaling/Brønsted–Evans–Polanyi relations, J. Catal. 309 (2014) 248-259.

[54] A. Vojvodic, F. Calle-Vallejo, W. Guo, S. Wang, A. Toftelud, J. I. Martinez, J. Shen, I. C. Man, J. Rossmeist, T. Bligaard, J. K. Norskov, F. Abild-Pedersen, On the behavior of Brønsted-Evans-Polanyi relations for transition metal oxides, J. Phys. 134 (2011), 244509-244517.

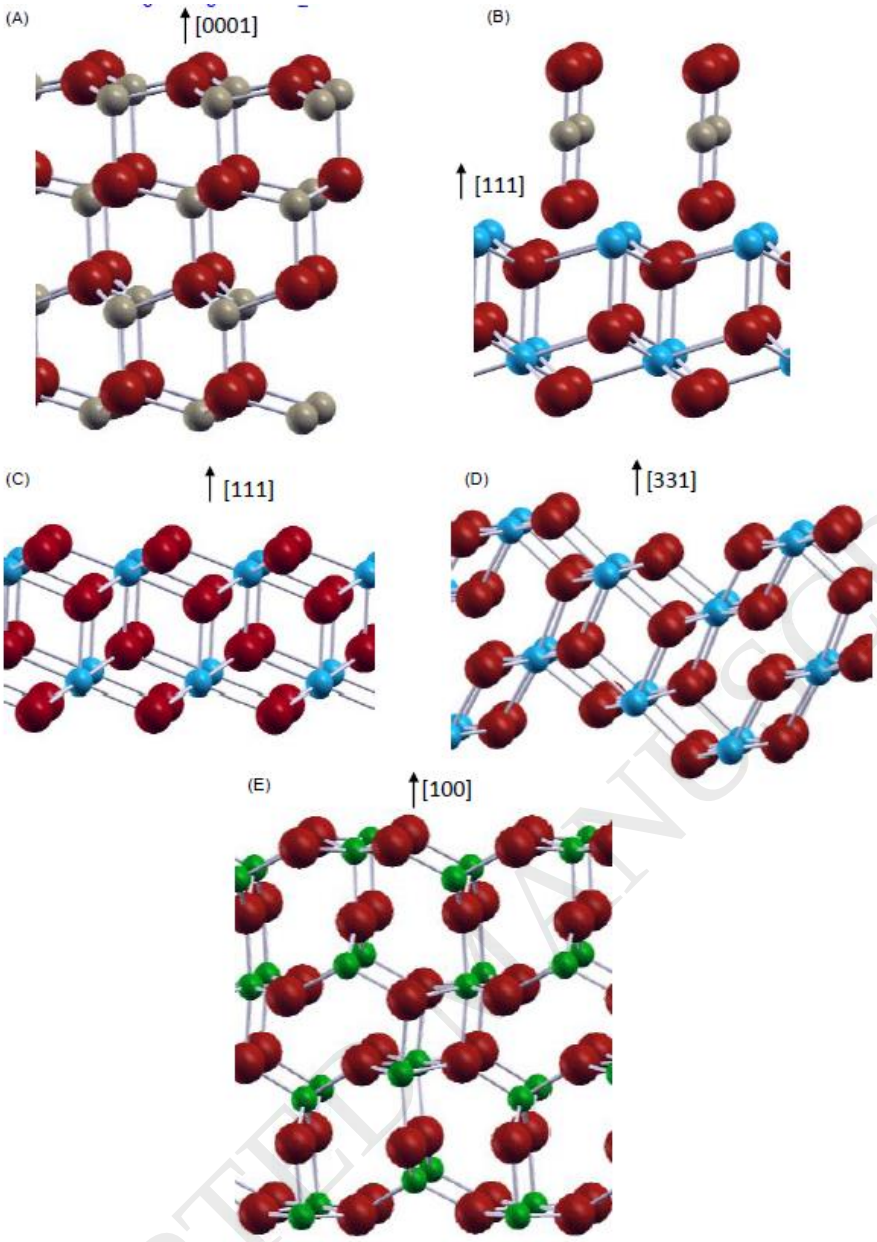

Figure 1: Pristine surfaces of (A) ZnO (0001), (B) ZnO/CeO_2 (111), (C) CeO_2 (111), (D) CeO_2 (331), and (E) Ga_2O_3 (100). Grey spheres: Zn atoms, blue spheres: Ce atoms, red spheres: O atoms, and green spheres: Ga atoms.

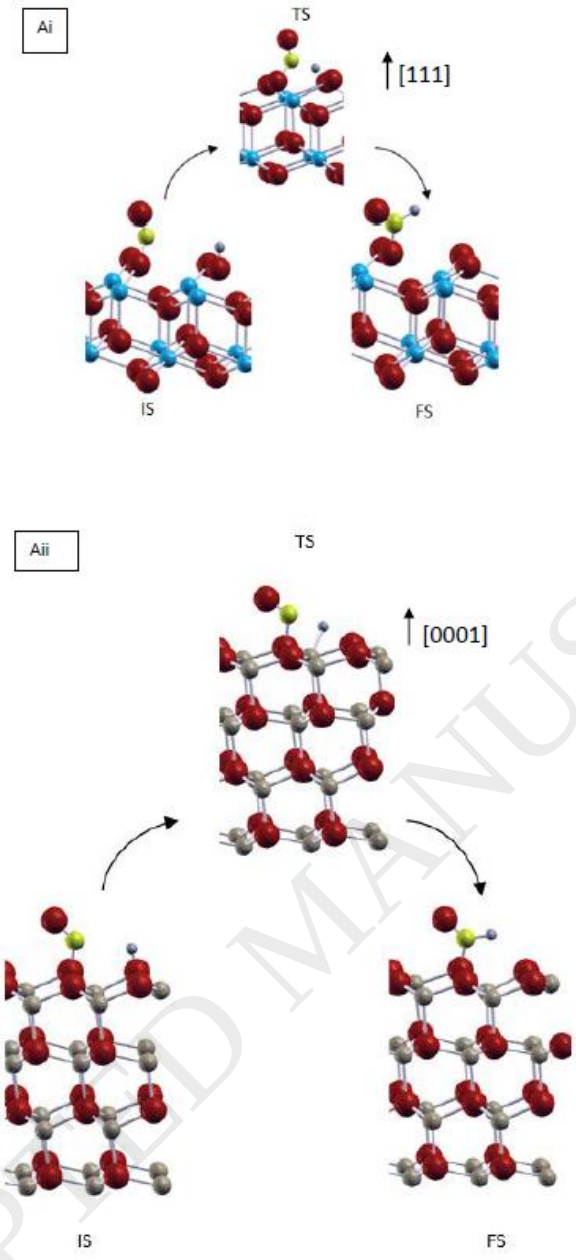

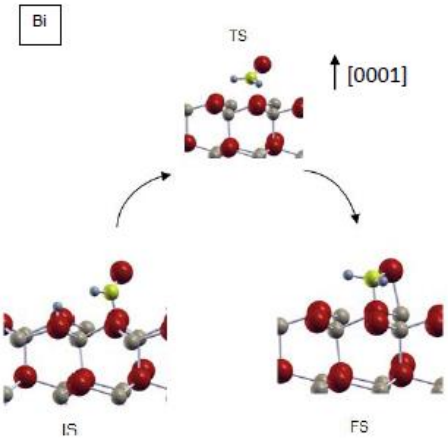

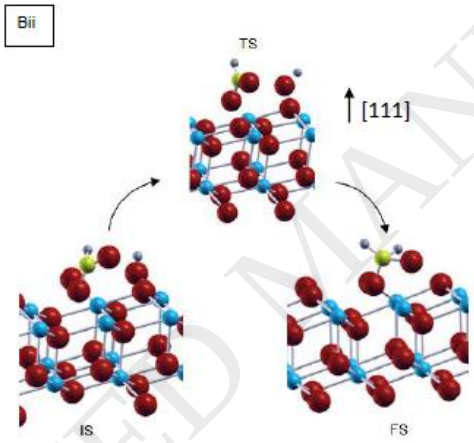

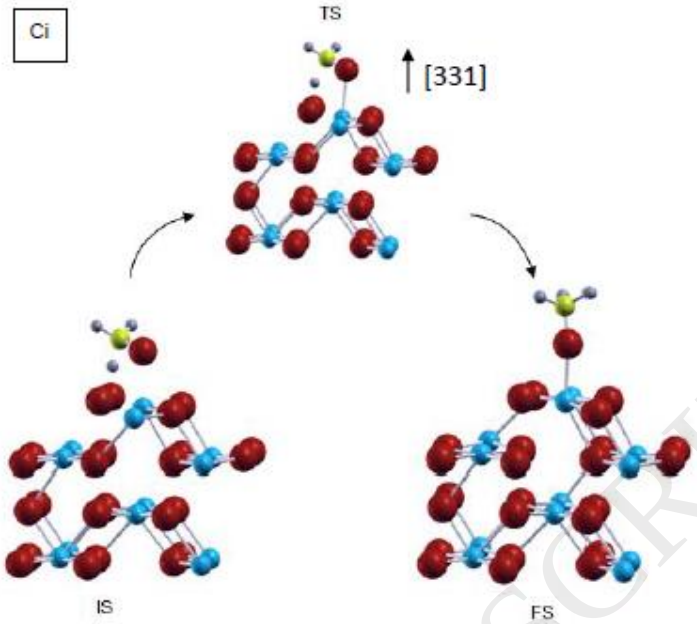

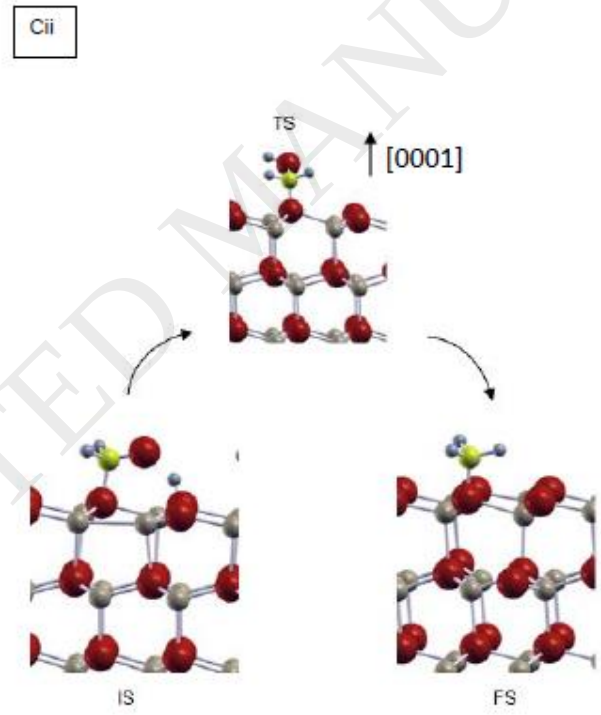

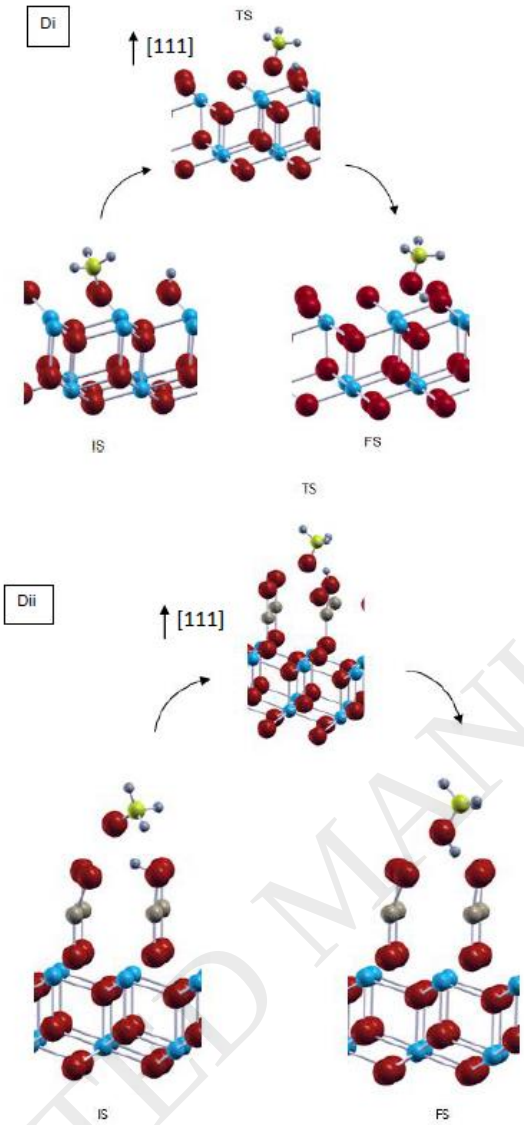

Figure 2: Representative hydrogenation reaction steps to produce adsorbed intermediates on the different studied surfaces: (Ai) Formyl on CeO_2 (111). (Aii) Formyl on ZnO (0001). (Bi) Formaldehyde on ZnO (0001). (Bii) Formaldehyde on CeO_2 (111)vacO. (Ci) Methoxy on CeO_2 (331). (Cii) Methoxy on ZnO (0001)vacO. (Di) Methanol on CeO_2 (111). (Dii) Methanol on ZnO/CeO_2 (111). IS: initial state - TS: transition state - FS: final state.

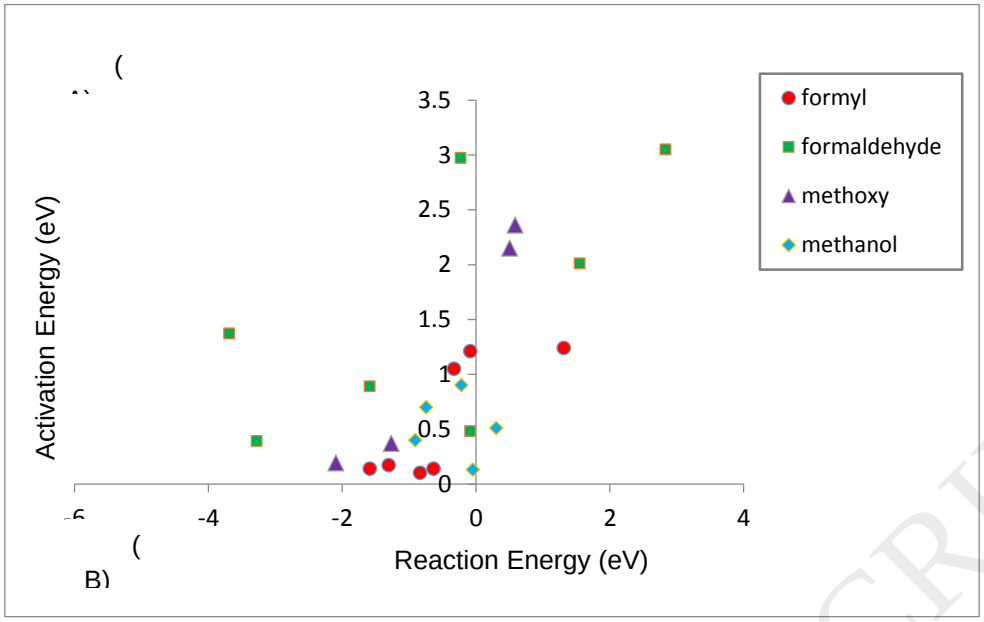

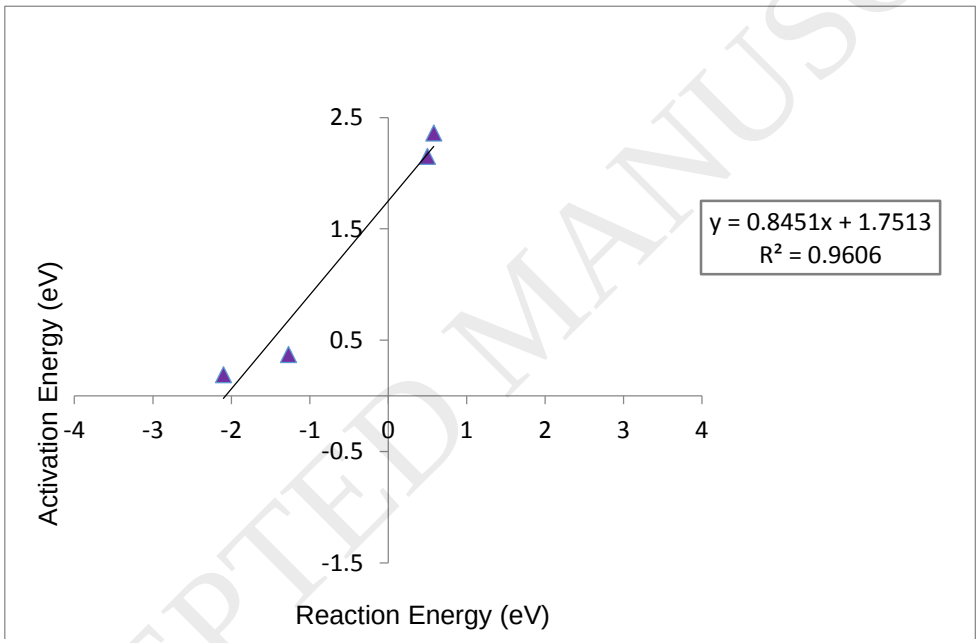

Figure 3: (A) Traditional Brønsted–Evans–Polanyi (BEP) relation for the activation energy vs the hydrogenation reaction energy for all the reactions on the different studied surfaces. (B) Traditional BEP for the activation energy vs the hydrogenation reaction energy for methoxy formation.

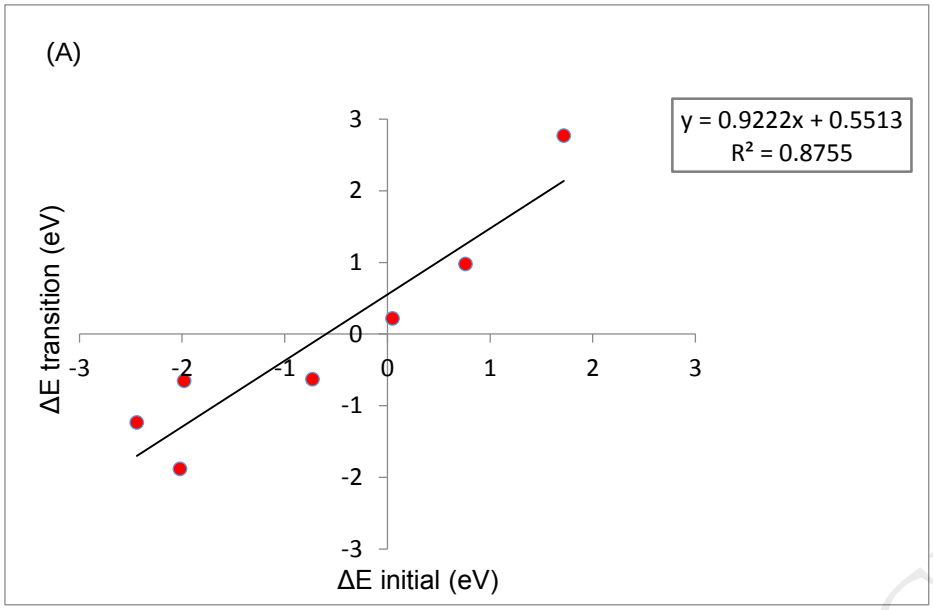

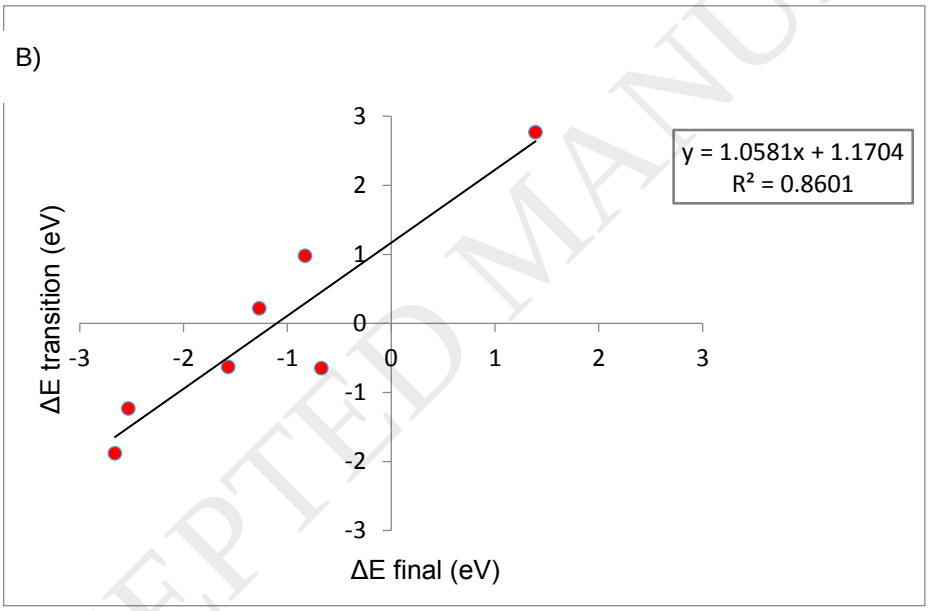

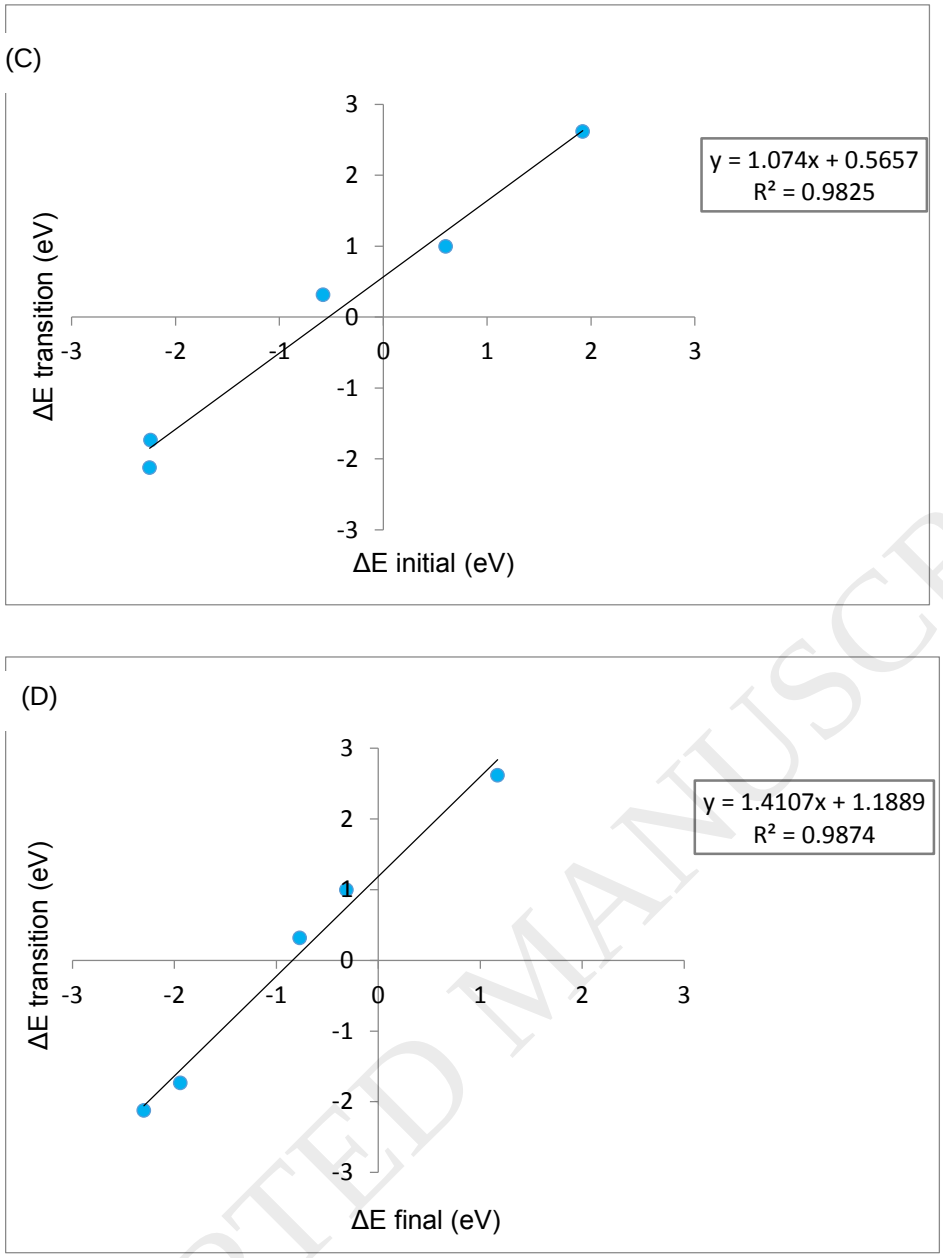

Figure 4: Brønsted–Evans–Polanyi (BEP) relation for the activation energy for formyl formation (HCO) vs the: (A) ΔE initial state and (B) ΔE final state. BEP relation for the activation energy for methanol formation (H_3COH) vs the: (C) ΔE initial state and (D) ΔE final state.

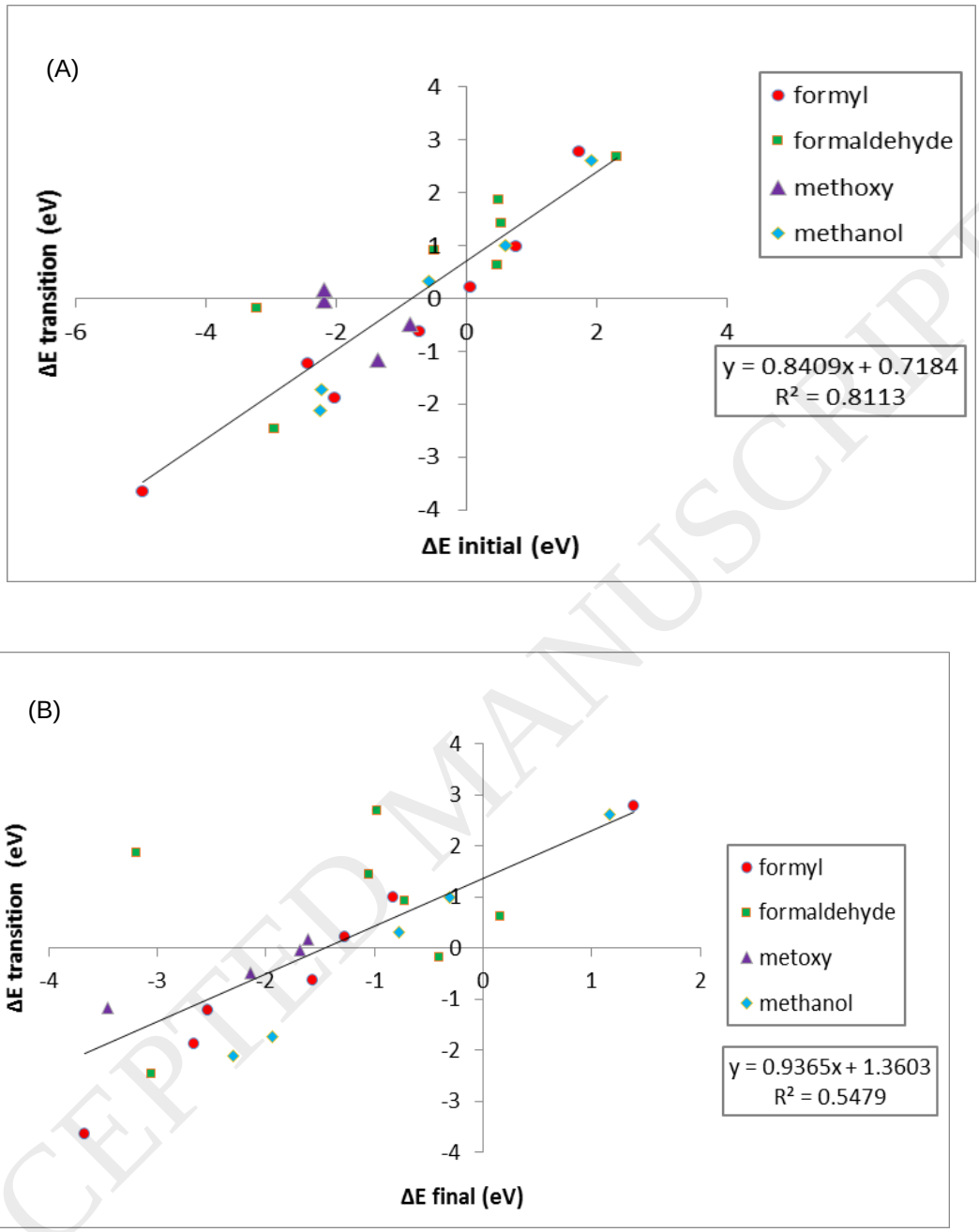

Figure 5: Brønsted–Evans–Polanyi (BEP) relation for all the reactions for the activation energy vs the: (A) ΔE initial state and (B) ΔE final state.

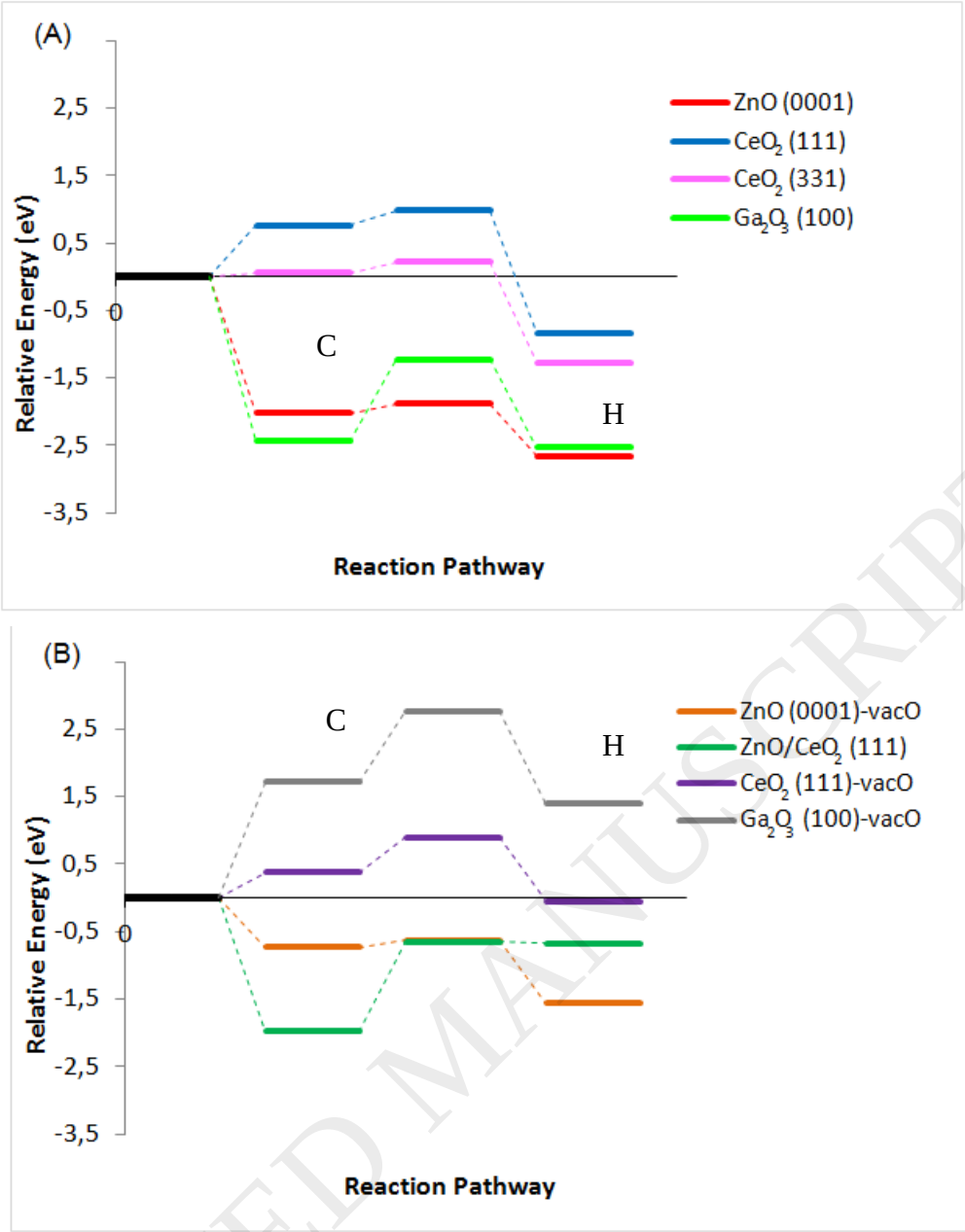

Figure 6: Formyl formation from CO and H on (A) ZnO (0001), CeO_2 (111), CeO_2 (331), Ga_2O_3 (100), (B) ZnO (0001)-vacO, ZnO/CeO_2 (111), CeO_2 (111)-vacO and Ga_2O_3 (100)-vacO.

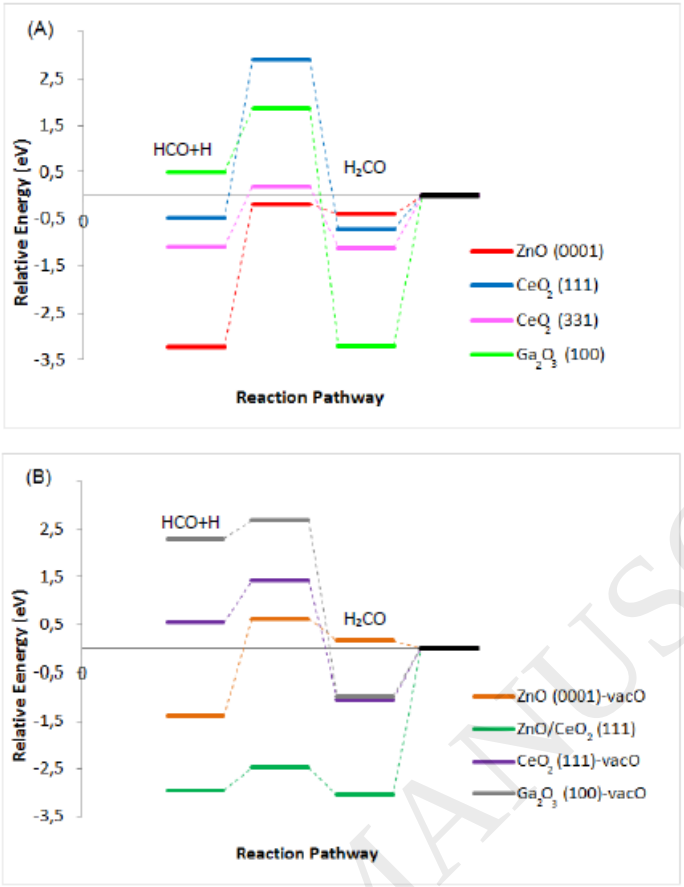

Figure 7: Formaldehyde formation from formyl on: (A) ZnO (0001), CeO_2 (111), CeO_2 (331), Ga_2O_3 (100). (B) ZnO (0001)-vacO, CeO_2 (111)-vacO, Ga_2O_3 (100)-vacO and ZnO/CeO_2 (111).

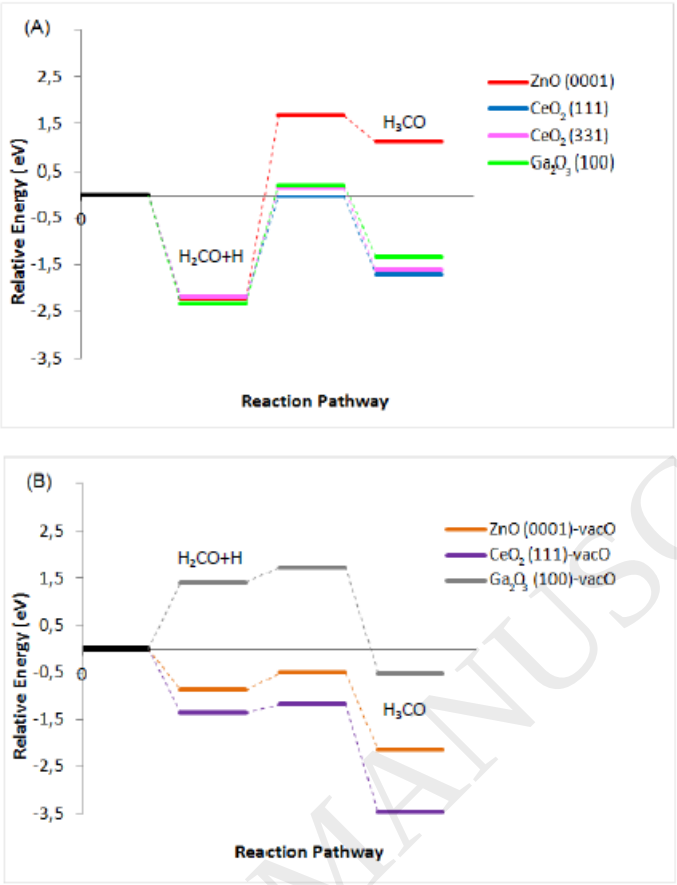

Figure 8: Metoxy formation from formaldehyde on: (A) ZnO (0001), CeO_2 (111), CeO_2 (331), Ga_2O_3 (100). (B) ZnO (0001)-vacO, CeO_2 (111)-vacO, Ga_2O_3 (100)-vacO.

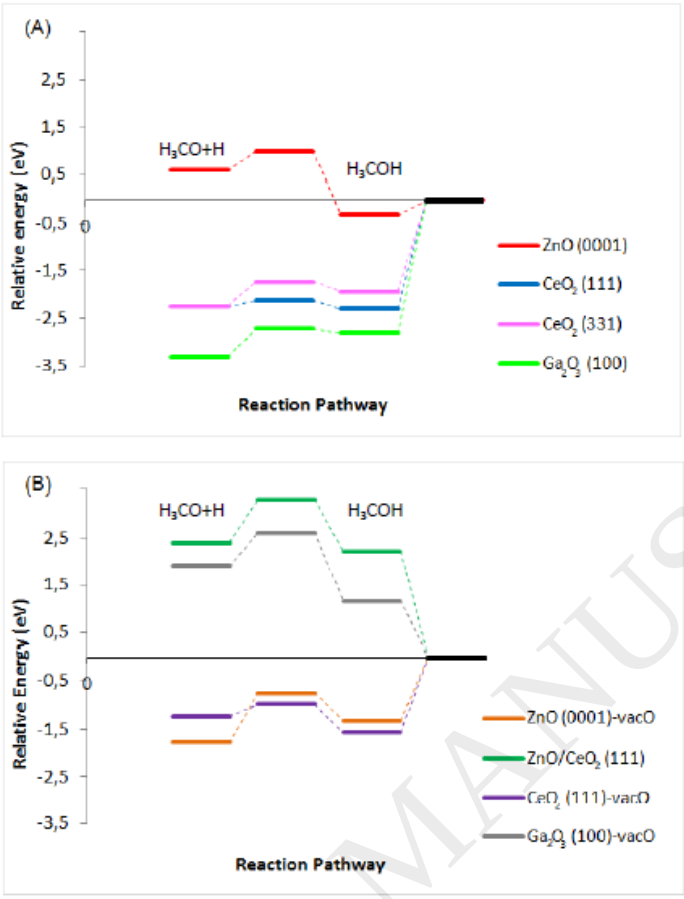

Figure 9: Methanol formation from methoxy on: (A) ZnO (0001), CeO_2 (111), CeO_2 (331), Ga_2O_3 (100). (B) ZnO (0001)-vacO, ZnO/CeO_2 (111), CeO_2 (111)-vacO and Ga_2O_3 (100)-vacO.

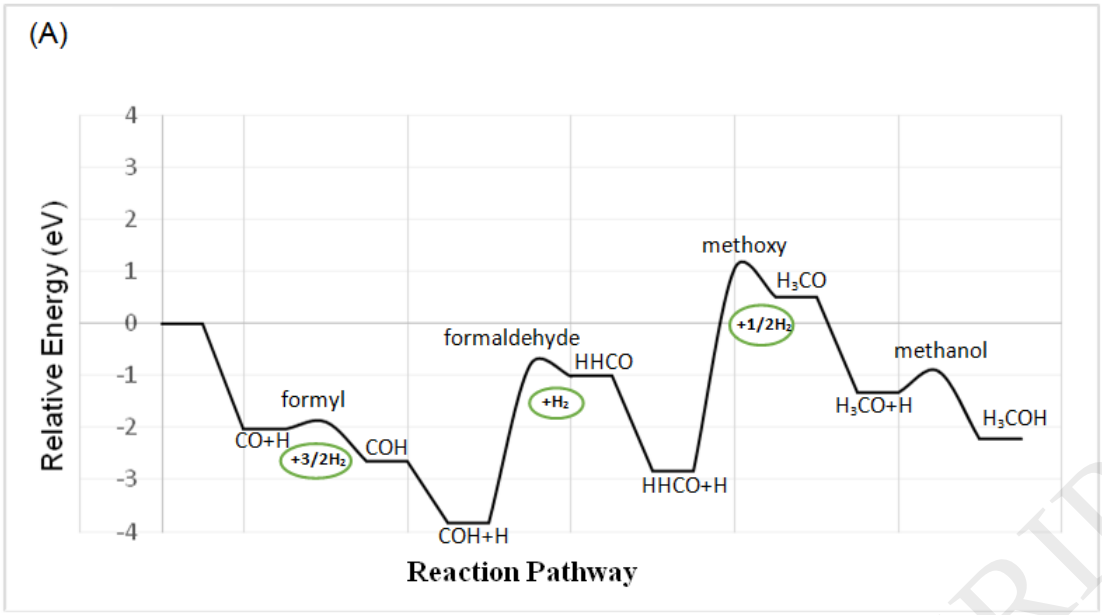

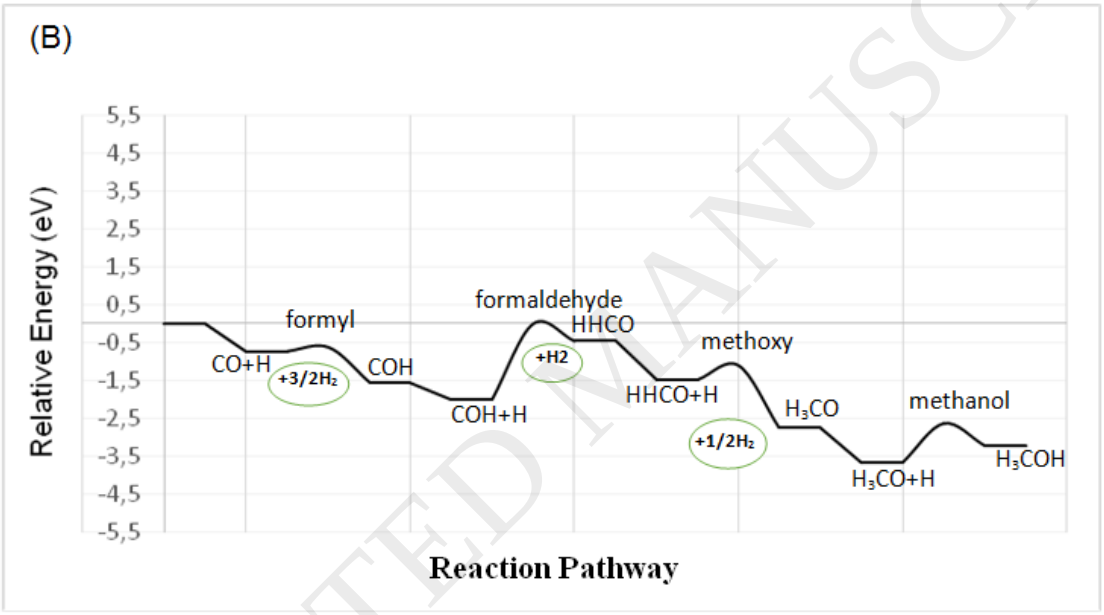

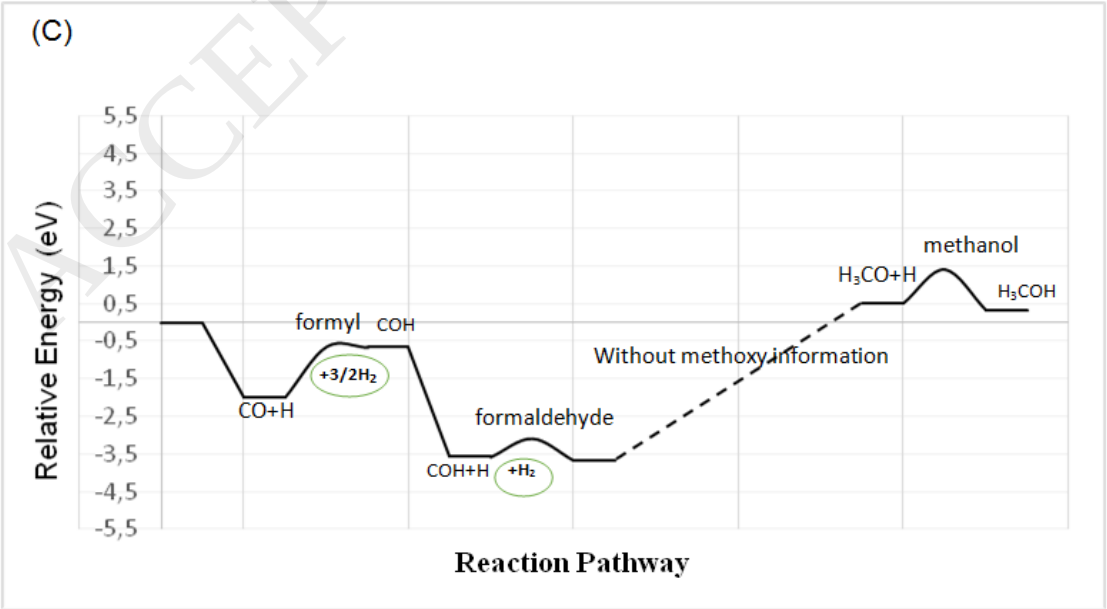

Figure 10: Relative energy diagram for the hydrogenation of CO to methanol on: (A) ZnO (0001). (B) ZnO (0001)-vacO, and (C) ZnO/CeO_2 (111).

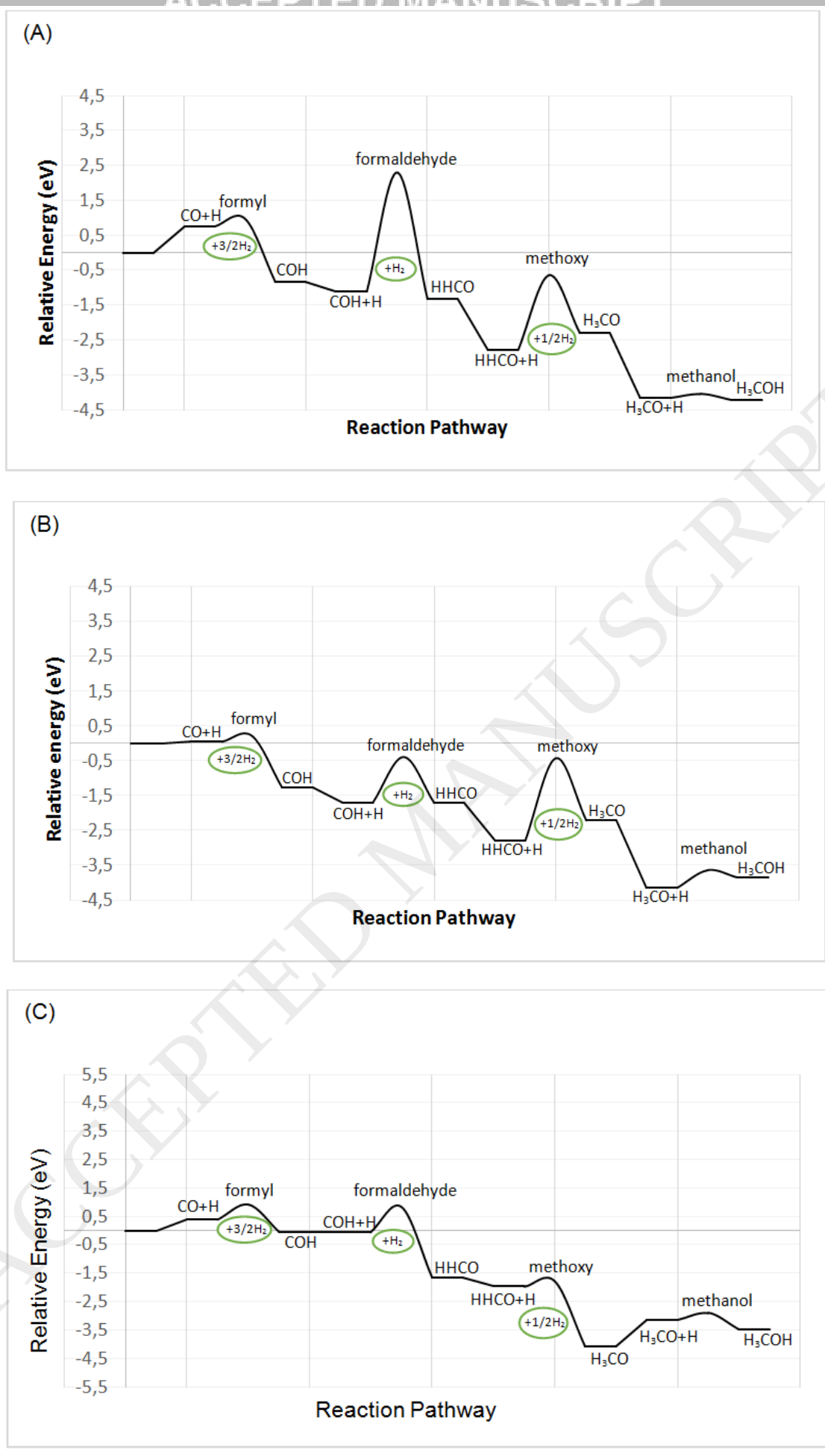

Figure 11: Relative energy diagram for the hydrogenation of CO to methanol on: (A) CeO_2 (111). (B) CeO_2 (331), and (C) CeO_2(111)-vacO.

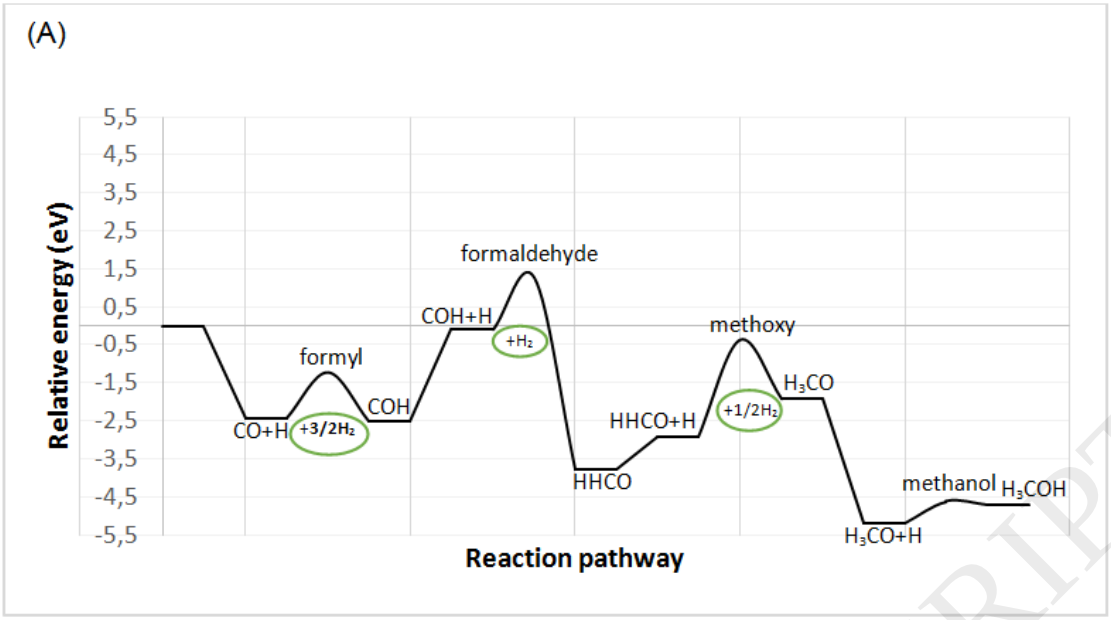

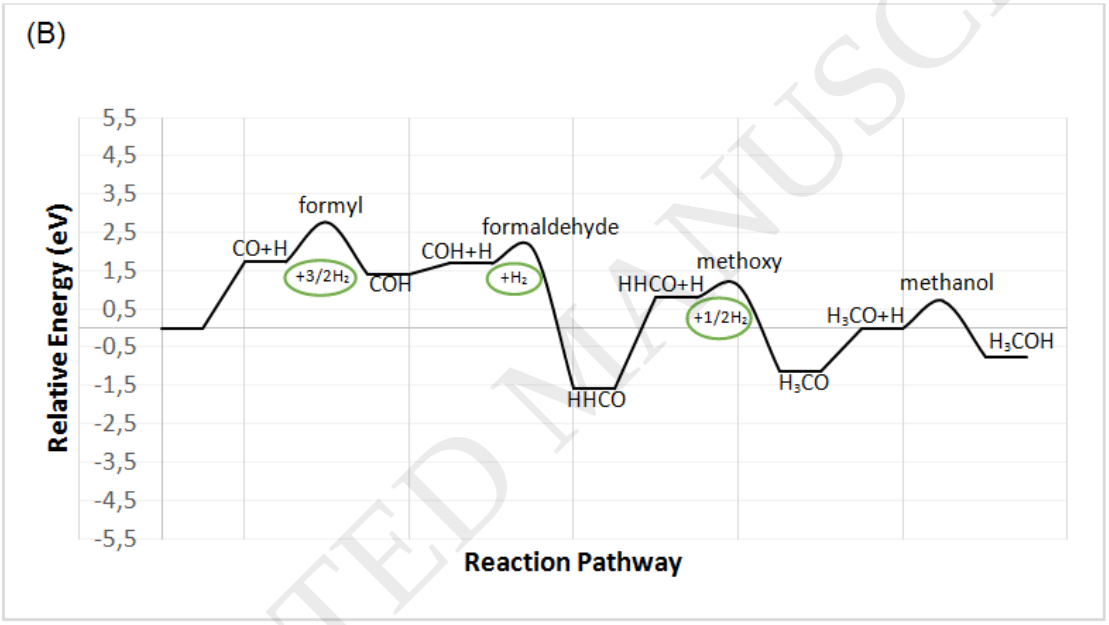

Figure 12: Relative energy diagram for the hydrogenation of CO to methanol on: (A) Ga_2O_3 (100) and (B) Ga_2O_3 (100)-vacO.